Earth and Planetary Science Letters 510 (2019) 53–63

Contents lists available at ScienceDirect

Earth and Planetary Science Letters

www.elsevier.com/locate/epsl

Increased export production during recovery from the Paleocene–Eocene thermal maximum constrained by sedimentary Ba isotopes

Luke Bridgestock *, Yu-Te Hsieh, Donald Porcelli, Gideon M. Henderson

Department of Earth Science, University of Oxford, South Parks Road, Oxford, OX1 3AN, UK

ARTICLE INFO

Article history:
Received 1 September 2018
Received in revised form 18 December 2018
Accepted 28 December 2018
Available online 17 January 2019
Editor: D. Vance

Keywords:
Ba isotopes
export production
Paleocene–Eocene thermal maximum
Ba accumulation rates

ABSTRACT

The Paleocene–Eocene thermal maximum (PETM; ~56 Ma) was a transient global warming event associated with a huge perturbation to the global carbon cycle. Changes in marine biological productivity may have contributed to the rapid recovery from this climate change event, by driving the burial of inorganic and organic carbon. Disagreement between proxy reconstructions, however, makes the response of biological productivity to climatic changes experienced during the PETM uncertain. Accumulation of non-detrital barium (Ba) in marine sediments is a commonly used proxy for export production. This proxy however can be compromised by artifacts resulting from dilution and changes in barite preservation, issues that have been debated for its application to sediments deposited during the PETM. Here we present a new approach to address these limitations, by combining non-detrital Ba accumulation with Ba isotope data for marine PETM sediments. Observed positive correlation between these variables is consistent with their control by local changes in export production. These results help resolve previous discrepancies between productivity reconstructions, and indicate export production at sites in the Southern Ocean and South Atlantic decreased or remained unchanged following the PETM onset, followed by an increase to maximum values in the PETM recovery period. This increase in export production coincides with elevated carbonate accumulation rates, representing an important mode of carbon sequestration. These new constraints therefore support the idea that increased production and export of calcifying nannoplankton, perhaps driven by changes in ocean stratification and/or terrestrial runoff, played an important role in rapid recovery from the PETM. This work also demonstrates the utility of sedimentary Ba isotope compositions for understanding past changes in the marine carbon cycle.

1. Introduction

The Paleocene–Eocene thermal maximum (PETM; ~56 Ma) was an abrupt period of climate change, associated with a large perturbation to the carbon cycle and a global sea-surface-temperature rise of at least 4 to 5 °C (McInerney and Wing, 2011; Dunkley Jones et al., 2013). The onset of the PETM is marked by a negative carbon isotope excursion in sedimentary records, reflecting release of a huge amount of ^{13}C-depleted carbon to the ocean and atmosphere (McInerney and Wing, 2011). About 100 kyrs after the event onset (Murphy et al., 2010; Westerhold et al., 2018), $^{13}C/^{12}C$ ratios of sedimentary components recover towards pre-event values, representing the sequestration of this excess carbon (Kelly et al., 2005). Enhanced silicate weathering and resulting carbonate burial is invoked as the main mechanism for this recovery (Kelly et al., 2005; Zachos et al., 2005; Penman et al., 2016), although its rapidity also requires significant amounts of carbon sequestration in organic carbon reservoirs (Bowen and Zachos, 2010; Gutjahr et al., 2017; Komar and Zeebe, 2017).

Marine biological productivity may have contributed to CO_2 sequestration during the PETM by driving burial of inorganic and organic carbon (Bains et al., 2000; Kelly et al., 2005; Gibbs et al., 2006, 2018; Stoll et al., 2007; Ma et al., 2014; Komar and Zeebe, 2017). The potential drivers of productivity changes in response to climatic change experience during the PETM are numerous and likely to vary both geographically and temporally. In continental shelf settings, productivity generally increased following the PETM onset in response to higher nutrient supply due to terrestrial runoff (Gibbs et al., 2006; Carmichael et al., 2017). Away from continental shelves, productivity may have been influenced by changes in water column stratification (Gibbs et al., 2006; Winguth et al., 2012), in addition to ocean pH changes that may

* Corresponding author.
E-mail address: luke.bridgestock@earth.ox.ac.uk (L. Bridgestock).

https://doi.org/10.1016/j.epsl.2018.12.036
0012-821X/

have affected calcifying phytoplankton (Zachos et al., 2005). Lack of consensus between different proxy reconstructions however, has hindered understanding of productivity changes in off-shelf settings during the PETM.

Key evidence for changes in the production and export of particulate organic carbon from the surface ocean (export production) during the PETM is based on the accumulation rate of non-detrital barium (Ba) or barite ($BaSO_4$) in marine sediments (Bains et al., 2000; Ma et al., 2014). These studies suggest that export production increased at off-shelf sites throughout the ocean following the PETM onset before declining during the recovery from the PETM. These inferred changes however seem at odds with interpretations of biotic proxies at the same locations. For example, at Ocean Drilling Program (ODP) Site 690 (Southern Ocean) evidence from nannofossils has been interpreted to reflect decreased nutrient supply following the PETM onset, increasing during the recovery period (Bralower, 2002), associated with higher production and export of calcareous nannoplankton (Kelly et al., 2005; Gibbs et al., 2018). Alternatively, nannofossil evidence has also been interpretation to represent constant biogenic carbonate production and export throughout the PETM at this site (Gibbs et al., 2010). Both of these interpretations significantly disagree with inferred changes in organic carbon production and export at this site using the Ba proxy (Bains et al., 2000; Ma et al., 2014).

Disagreement between productivity reconstructions may stem from two issues related to the application of the Ba proxy. First, changes in sediment Ba concentrations during the PETM are influenced by variable dilution by carbonate minerals (Torfstein et al., 2010), in turn related to changes in ocean pH (Zachos et al., 2005). Disagreement between reconstructions of bulk sedimentation rate makes accurately accounting for these dilution effects problematic (Farley and Eltgroth, 2003; Murphy et al., 2010; Murphy, 2011; Westerhold et al., 2018). The second issue is that non-detrital Ba accumulation may be influenced by changes in $BaSO_4$ preservation as well as export production. The destabilization of seafloor methane hydrates, a proposed source of the additional ^{13}C-depleted carbon released during the PETM (Dickens et al., 1995), may also have released large amounts of Ba to the ocean at the onset of the event (Dickens et al., 2003). This would act to shift the deep ocean closer to $BaSO_4$ saturation, potentially increasing $BaSO_4$ preservation rates and is suggested as an alternative explanation for high Ba accumulation rates following the PETM onset (Dickens et al., 2003).

Here we present the first paleo-oceanographic application of sedimentary Ba isotope compositions. Barium isotope compositions of marine sediments have recently been proposed as a novel tool to gain insights into the cycling of Ba in the upper ocean that should be insensitive to variations in dilution and $BaSO_4$ preservation (Bridgestock et al., 2018). Combined records of sedimentary non-detrital Ba accumulation and Ba isotope composition may provide more robust constraints on export production during the PETM and enable the mechanisms contributing to recovery from this abrupt climate change event to be understood.

2. Samples

The sediment samples used in this study were obtained from ODP Sites 690 (65°9.621′S, 01°12.285′E) and 1263 (28°31.98′S, 02°46.77′E) (Fig. 1). Sediments deposited during the PETM at these sites have previously been the subject of export production reconstructions using the Ba proxy (Bains et al., 2000; Ma et al., 2014). Interpretations of productivity changes based on nannofossils are also available for ODP Site 690 (Bralower, 2002; Kelly et al., 2005; Gibbs et al., 2010, 2018), allowing direct comparison of results from this study to wider constraints. These cores are also among the only ones for which there are age models and sedimentation

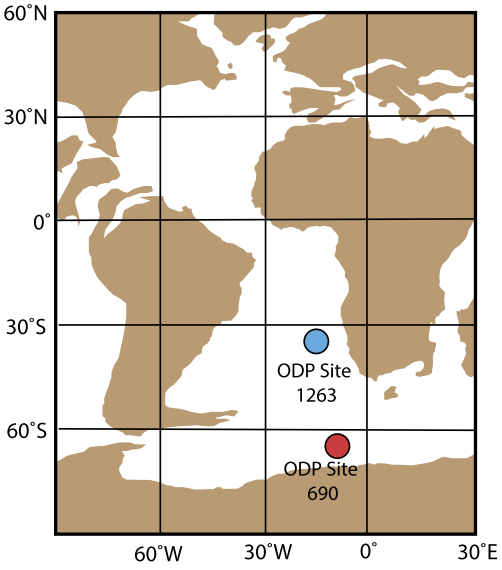

Fig. 1. Map showing the locations of the studied sediment cores in context of a reconstruction of the paleogeography during the Paleocene–Eocene thermal maximum. The map was generated using the Ocean Drilling Stratigraphic Network (http://www.odsn.de/odsn/index.html).

rate estimates across the PETM based on both cyclostratigraphy and extraterrestrial ^{3}He (Farley and Eltgroth, 2003; Murphy, 2011; Westerhold et al., 2018). This allows comparison of non-detrital Ba accumulation rates calculated using independent assessments of changes in dilution. In addition, $BaSO_4$ separated from these sediments has been previously found to show no evidence for diagenetic alteration (Ma et al., 2014), making them an ideal target for this study.

3. Methods

Concentrations of Ba and Al, and Ba isotope compositions were determined for total sediment digestions of 45 samples across the PETM from ODP Sites 690 and 1263. Approximately 1 cc of sediment was crushed and homogenized by pestle and mortar, and 0.1 to 0.2 g of powdered sediment was weighed, prior to total digestion following established protocols (Homoky et al., 2011; Bridgestock et al., 2018). Aliquots of the digested solutions were taken for measurement of Al concentrations using quadrupole inductively coupled plasma mass spectrometry (6100DRC; Perkin Elmer). Measurements of Ba concentrations and isotope compositions were conducted using thermal ionization mass spectrometry (TIMS; TRITON instrument, Thermo Scientific). Aliquots of the digested solutions containing about 2 µg of Ba were equilibrated with a known quantity of a Ba double spike solution (Hsieh and Henderson, 2017), before processing through an ion exchange chromatography procedure (Hsieh and Henderson, 2017; Bridgestock et al., 2018). The procedural blank was between 0.2 and 2.6 ng of Ba ($n = 6$) representing <0.13% of the Ba processed in the samples, with the exception of a single batch of processed samples for which the blank was 86 ng of Ba. Repeat measurements of select samples from this batch indicate no significant impact on data quality due to this higher level of blank (representing 4.3% of the Ba processed in the samples), so no blank corrections were applied.

Barium isotope measurements using TIMS featured a double Re filament assembly, with the purified Ba from the samples loaded onto the evaporation filament in 2M HCl without an activator gel. Barium ionization was achieved by applying currents of 2000 to 2500 mA to the ionization filament and 50 to 300 mA to the

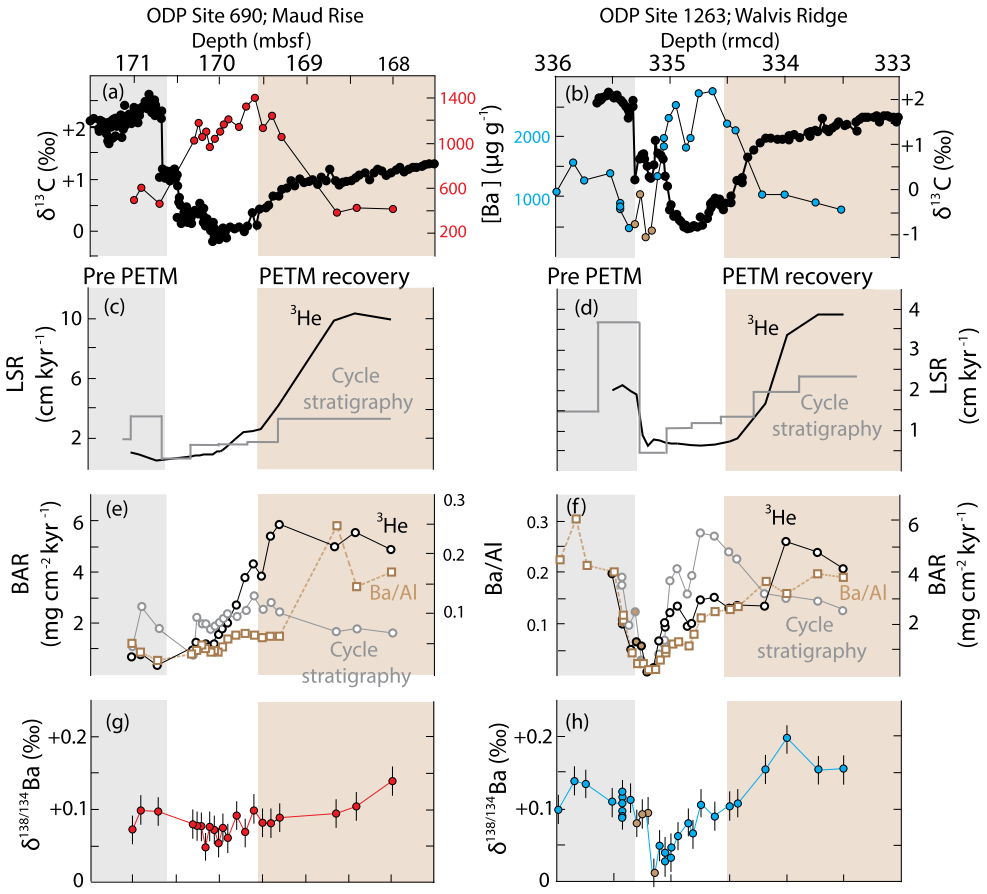

Fig. 2. Total Ba concentrations, isotope compositions and accumulation indices across the PETM at ODP sites 690 and 1263. Panels (a) and (b) display carbon isotope compositions (black circles; Bains et al., 1999: Zachos et al., 2005), and Ba concentrations determined in this study (red and blue circles). Panels (c) and (d) show reconstructions of linear sedimentation rates (LSR) derived using cycle stratigraphy (grey lines; Westerhold et al., 2018) and extraterrestrial ^{3}He (black lines; Farley and Eltgroth, 2003; Murphy, 2011). Panels (e) and (f) display Ba/Al ratios and (non-detrital) Ba accumulation rates (BAR) calculated using the two LSR estimates shown in panels (c) and (d). Panels (g) and (h) show Ba isotope composition results determined in this study. For ODP site 1263, solid brown circles indicate samples that are significantly impacted by Ba contributions from detrital sources. The depth scales denote meters below seafloor (mbsf) and revised meters composite depth (rmcd) (For interpretation of the colors in the figure(s), the reader is referred to the web version of this article.).

evaporation filament. Stable ion-beam intensities of about 10 V for ^{138}Ba were achieved, and isotopic ratios were measured following previously described protocols (Hsieh and Henderson, 2017). Instrumental mass bias corrected Ba isotope ratios were calculated offline and Ba concentrations were calculated by isotope dilution. Barium isotope compositions are expressed as $\delta^{138/134}$Ba values (1) relative to the standard reference material NIST 3104a.

$$\delta^{138/134}\text{Ba‰} = \left(^{138}\text{Ba}/^{134}\text{Ba}_{\text{sample}}/^{138}\text{Ba}/^{134}\text{Ba}_{\text{NIST3104a}} - 1\right) \times 1000 \quad (1)$$

Repeat measurements of the inter-laboratory Ba standard, BaBe 27, conducted every measurement session, and a single measurement of the inter-laboratory Ba standard, BaBe 12, yielded $\delta^{138/134}\text{Ba} = -0.82 \pm 0.02$‰ (mean ±2sd, $n = 9$) and $\delta^{138/134}\text{Ba} = -1.51$‰ respectively, in excellent agreement with published values ($\delta^{138/134}\text{Ba} = -0.82 \pm 0.03$‰; $\delta^{138/134}\text{Ba} = -1.54 \pm 0.03$‰; van Zuilen et al., 2016). Aliquots of a sediment digest (ODP Site 1263; 335.42 revised meters composite depth) were processed through the chemical separation procedure and measured with every batch of samples processed, yielding $\delta^{138/134}\text{Ba} = 0.10 \pm 0.02$‰ (mean ±2sd, $n = 6$) (Fig. 2; Supplementary Data). This level of reproducibility is taken to represent that of the other samples, which is justified by the agreement of duplicate analyses of select samples.

4. Results

The sampled core intervals are divided into three sections based on bulk carbon isotope variations: a pre-PETM period, the onset and main period of the PETM, and a period of recovery from the PETM (Fig. 2; Bains et al., 1999; Zachos et al., 2005). Determined total Ba concentrations range from 333 to 2741 μg g^{-1}, in good agreement with literature data from ODP Site 690 (Fig. 3; Supplementary Data) (Bains et al., 2000). Following the onset of the PETM, Ba concentrations increase at both sites before decreasing during the recovery period. At ODP Sites 690 and 1263, pre-PETM samples display $\delta^{138/134}$Ba values of +0.10‰ (Fig. 2), similar to those reported for modern South Atlantic sediments (Bridgestock et al., 2018). At Site 690, $\delta^{138/134}$Ba values display a subtle decrease to +0.07 ± 0.01‰ (mean ±2SE; $n = 12$) following the PETM onset, before increasing to a maximum of +0.14‰ during the recovery period. A similar but more pronounced pattern is observed at Site 1263, where $\delta^{138/134}$Ba values decrease to +0.01‰ following the PETM onset, increasing to a maximum of +0.20‰ during the recovery period.

5. Discussion

The use of sedimentary Ba accumulation rates as a proxy for past changes in export production is based on the dominant removal flux of Ba from the water column to marine sediments

being through the precipitation of $BaSO_4$. This is thought to occur in microenvironments associated with the decomposition of organic matter in the upper water column (Dehairs et al., 1980). Fluxes of particulate organic carbon and Ba sinking through the water column are typically correlated (e.g. Dymond et al., 1992), so that Ba accumulation rates in underlying sediments should be proportional to export production. Like all paleo-productivity proxies however, other processes can influence the accumulation of Ba in sediments, compromising the reliability of export production reconstructions. On average about ~70% of the $BaSO_4$ delivered to the seafloor will re-dissolve (Paytan and Kastner, 1996), and changes in $BaSO_4$ preservation can influence Ba accumulation rates in marine sediments independently from export production (Fagel et al., 2002). The exact controls on $BaSO_4$ preservation in marine sediments are poorly known, although bottom water $BaSO_4$ saturation state and sedimentation rate are proposed as important variables (Dymond et al., 1992; Fagel et al., 2002). Furthermore, dilution effects due to bulk sedimentation rate changes can be difficult to account for, affecting the accuracy of calculated Ba accumulation rates. Finally marine sediment may receive significant inputs of Ba from phases that are unrelated to export production such as inputs of detrital aluminosilicate minerals (Klump et al., 2000; Reitz et al., 2004). These complications need to be accounted for to enable reliable reconstructions of export production using this proxy.

The assessment of Ba inputs to marine sediments from different phases has received considerable attention (Klump et al., 2000; Rutten and de Lange, 2002; Reitz et al., 2004; Eagle et al., 2003; Gonneea and Paytan, 2006), however reliable approaches to identify and account for dilution and preservation issues are currently lacking. During periods of dramatic climatic change, rapid changes in sedimentation rate are common, and factors such as bottom water $BaSO_4$ saturation state could vary. This emphasizes the need for an approach to reliably account for $BaSO_4$ preservation and dilution effects to enable robust export production reconstructions. The application of this proxy to the PETM is a prominent example where these issues have been debated (Dickens et al., 2003; Paytan et al., 2007; Torfstein et al., 2010).

In the following we assess the importance of different phases for hosting Ba in the studied core intervals (section 5.1), before using three independent techniques to estimate changes in non-detrital Ba accumulation (section 5.2). We then introduce Ba isotopes as a new tool to study the cycling of this element in the ocean, and outline a framework in which to interpret the $\delta^{138/134}$Ba values recorded by marine sediments (section 5.3). Finally we interpret the non-detrital Ba accumulation and $\delta^{138/134}$Ba records in the context of export production, dilution artifacts and $BaSO_4$ preservation issues (section 5.4), and discuss our interpretations of export production in context of wider constraints for the PETM (section 5.5).

5.1. Which phase hosts Ba in analyzed sediments?

Contributions of Ba to marine sediment by phases other than $BaSO_4$ can compromise the accuracy of export production using sedimentary Ba accumulation rates (Dymond et al., 1992; Eagle et al., 2003). Association of Ba with different phases will also affect interpretations of $\delta^{138/134}$Ba values of bulk sediment. In addition to $BaSO_4$, Ba can be associated with detrital aluminosilicate minerals, carbonate minerals, organic matter and Fe–Mn oxyhydroxide phases (Dymond et al., 1992; Eagle et al., 2003; Gonneea and Paytan, 2006).

Contributions of Ba from detrital inputs can be quantitatively assessed by assuming a Ba/Al ratio for the detrital component of the sediment (2).

$$Ba_{Detrital}\ (\%) = (Ba/Al_{Detrital} \times Al_{Total})/Ba_{Total} \times 100 \quad (2)$$

where $Ba_{Detrital}$ denotes Ba from detrital sources, Ba_{Total} and Al_{Total} denote the total Ba and Al concentrations of the sediment, and $Ba/Al_{Detrital}$ denotes the reference ratio of the detrital material. The accuracy of these detrital Ba estimates depends on the choice of $Ba/Al_{Detrital}$ reference ratios, which are known to vary regionally in the modern ocean (Klump et al., 2000; Reitz et al., 2004). In absence of direct constraints on the appropriate $Ba/Al_{Detrital}$ reference ratio for the studied PETM sediments, we assume 0.0037, which represents an estimate of the global average (Reitz et al., 2004). Detrital Ba contributions estimated using this ratio are typically <10% of the total Ba, with the notable exception of four samples immediately following the PETM onset from Site 1263, that range between 18% to 43% (Fig. 3). These four samples are from a clay-rich layer that formed due to the chemical erosion of carbonate minerals in response to ocean acidification at the onset of the PETM (Zachos et al., 2005). Due to the large detrital Ba contributions to these four samples, we exclude them from further discussion regarding past changes in the marine Ba cycle (section 5.4).

An upper limit on likely detrital Ba contributions can be assessed using $Ba/Al_{Detrital} = 0.0075$; the ratio in the upper continental crust (Dymond et al., 1992), which is considered to overestimate typical sedimentary $Ba/Al_{Detrital}$ ratios (Reitz et al., 2004). In this case, detrital Ba contributions are still less than 15% for most samples, ranging up to 30% for a few select samples (excluding the four samples immediately following the PETM onset at Site 1263). These values however are likely to overestimate detrital Ba contributions and detrital corrections assuming $Ba/Al_{Detrital} = 0.0037$ (Reitz et al., 2004) are used in the following discussion.

Inputs from detrital Ba can influence the $\delta^{138/134}$Ba values of bulk sediment and affecting interpretation of such records. Few constraints are currently available for the isotope composition of this detrital Ba. Bridgestock et al. (2018), inferred $\delta^{138/134}$Ba ≈ −0.1 to 0‰ for detrital Ba in modern sediments off the Uruguayan margin, in good agreement with the estimated average composition of the upper continental crust, of $\delta^{138/134}$Ba = 0.00 ± 0.04‰ (Nan et al., 2018). Assuming a range of detrital $\delta^{138/134}$Ba values (−0.1 to +0.1‰) alters the measured bulk sediment $\delta^{138/134}$Ba of most samples by <0.02‰ (i.e. the level of analytical uncertainty). Exceptions to this are a single sample from the pre-PETM interval from Site 690 (170.91 mbsf) that could be shifted by up to 0.04‰ and the four samples immediately following the PETM onset from Site 1263 that are estimated to have high detrital contributions. Excluding these five samples, we therefore consider detrital Ba inputs to have a negligible impact on the measured bulk sediment $\delta^{138/134}$Ba values.

A previous study directly measured $BaSO_4$ concentrations across the core intervals studied here by employing a sequential leaching procedure to separate $BaSO_4$ particles from other sedimentary components (Ma et al., 2014). Concentrations of Ba associated with this $BaSO_4$ (calculated by scaling $BaSO_4$ concentrations by 0.59) display broadly similar patterns to total Ba concentrations measured here but are between 32 and 95% lower (Fig. 3). It is possible that this discrepancy represents significant Ba contributions from other phases (carbonate, organic matter and/or Fe–Mn oxyhydroxides) in our record. As argued below however, the high total Ba concentrations of these sediments (333 to 2741 $\mu g\,g^{-1}$) are difficult to explain without large amounts of this Ba being supported by a minor Ba rich phase, most likely to be $BaSO_4$.

At both sites, carbonate minerals are the principal component of the sediment, with $CaCO_3$ concentrations ranging between 60 to 96 wt.% and 1 to 91 wt.% at Sites 690 and 1263 respectively (Fig. 3; Kelly et al., 2005; Zachos et al., 2005). Carbonate minerals are unlikely to be an important Ba-hosting phase in these sediments because they typically have low Ba contents of <70 $\mu g\,g^{-1}$

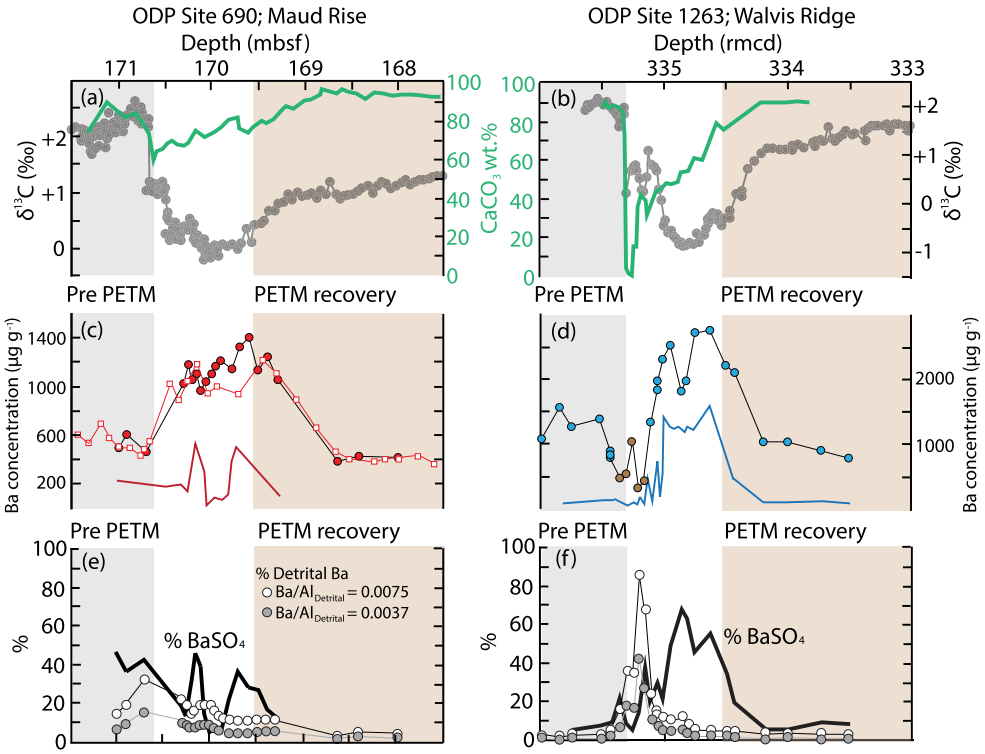

Fig. 3. Assessment of phases hosting Ba in studied sediment samples. Panels (a) and (b) display bulk $\delta^{13}C$ values (Bains et al., 1999; Zachos et al., 2005), and $CaCO_3$ concentrations of the sediments (Kelly et al., 2005; Zachos et al., 2005). Panels (c) and (d) display total Ba concentrations (filled circles – this study; open squares – Bains et al., 2000) and concentrations of Ba associated with $BaSO_4$ separated from the sediment using a sequential leaching procedure (red and blue lines; Ma et al., 2014). Panels (e) and (f) display estimated Ba contributions from detrital aluminosilicate minerals assuming $Ba/Al_{Detrital}$ reference ratios of 0.0075 and 0.0037 (2), Ba contributions from $BaSO_4$ separated from the sediment using a sequential leaching procedure (black lines; Ma et al., 2014). Depth scales denote meters below seafloor (mbsf) and revised meters composite depth (rmcd) for Sites 690 and 1263 respectively. (For interpretation of the colors in the figure(s), the reader is referred to the web version of this article.)

(Lea and Boyle, 1989; Gonneea and Paytan, 2006), and Ba concentrations in the sediment cores display a broadly antithetical relationship to $CaCO_3$, with carbonate acting as a diluent on Ba concentrations (Torfstein et al., 2010). To support the high total Ba concentrations of 333 to 2741 $\mu g\,g^{-1}$, large amounts of Ba must therefore be hosted by a minor Ba-rich phase. For example, samples from 334.18 to 333.50 rmcd at Site 1263, representing the PETM recovery period, are composed of about 90 wt.% $CaCO_3$ and have total Ba concentrations of about 1000 $\mu g\,g^{-1}$, of which only 2 to 5% is detrital (Fig. 3). The minor non-carbonate Ba hosting phase(s) in these samples must therefore have a Ba concentration of at least 1 wt.%. This amount of Ba cannot be supported by organic matter, which typically contains <300 $\mu g\,g^{-1}$ of Ba (Gonneea and Paytan, 2006), or Fe–Mn oxyhydroxides, which appear to be absent from this section of the core due to unfavorable redox conditions (Chun et al., 2010). It follows that the majority of the observed total Ba concentrations is most likely supported by $BaSO_4$. Direct measurements of $BaSO_4$ in this interval (Ma et al., 2014), however, suggest that only 10% of the Ba is in $BaSO_4$. It seems likely that this discrepancy, at least in part, reflects poor yields accompanying the leaching procedure used to separate $BaSO_4$ from the sediment (Ma et al., 2014). It has previously been suggested that this procedure is likely to be subject to such biases due to the partial dissolution and/or mechanical loss of $BaSO_4$ particles (Rutten and de Lange, 2002). Results of experiments to assess the $BaSO_4$ yield of this leaching procedure suggest that impact of poor $BaSO_4$ yields would increase with decreasing total $BaSO_4$ concentration (Eagle et al., 2003). It is therefore notable that the apparent fraction of Ba associated with $BaSO_4$ decreases with decreasing total Ba concentration (Fig. 3).

5.2. Estimating changes in non-detrital Ba accumulation

Three approaches are used to account for the effects of dilution and to convert Ba concentrations to Ba accumulation rates (BAR), as required for assessment of past export production. The first approach is to normalize Ba to Al concentrations in the sediments (Ba/Al ratios). In addition, two different estimates of BAR are calculated using independent published reconstructions of sedimentation rate. For calculation of BAR, total Ba concentrations are corrected for detrital contributions, assuming $Ba/Al_{Detrital} = 0.0037$ (Reitz et al., 2004) (2). Barium accumulation rates are then calculated using these detrital corrected Ba concentrations ($[Ba]_{xs}$), linear sedimentation rates (LSR), and sediment dry bulk densities (DBD) (3).

$$\mathrm{BAR}\left(\mathrm{mg\,cm^{-2}\,kyr^{-1}}\right) = \mathrm{LSR}\left(\mathrm{cm\,kyr^{-1}}\right) \times \mathrm{DBD}\left(\mathrm{g\,cm^{-3}}\right) \times [\mathrm{Ba}]_{\mathrm{xs}}\left(\mathrm{mg\,g^{-1}}\right) \quad (3)$$

For each site, estimates of LSR are derived using two age models, based on cyclostratigraphy (Westerhold et al., 2018) and extraterrestrial ^{3}He as a constant flux proxy (Fig. 2; Farley and Eltgroth, 2003; Murphy, 2011; Supplementary Information).

Results of each of these three approaches display different patterns of Ba accumulation across the studied core intervals (Fig. 2), highlighting the uncertainty on reconstruction of export production using the Ba proxy. Notably, BAR based on cyclostratigraphy age models increase to maxima at both sites following the PETM onset, before declining during the recovery period. In contrast, ^{3}He based BAR and Ba/Al ratios increase to maximum values in the PETM recovery period at both sites, although the exact timing and magnitude of these relative changes differ slightly between these two approaches.

These differences may be explained by the assumptions and uncertainty in the three approaches to assess changes in Ba accumulation. Cyclostratigraphic age models require the identification of cyclicity in sediment properties, which can be subjective, and are limited in resolution to the length of a processional cycle (in this case 21 kyr; Westerhold et al., 2018). The extraterrestrial ^{3}He method assumes a constant flux of extraterrestrial ^{3}He to the sediments so that its concentration is purely a function of bulk sedimentation rate (Farley and Eltgroth, 2003; Murphy, 2011; Murphy et al., 2010). The application of Ba/Al ratios assumes that Al is only associated with detrital aluminosilicate minerals, that the flux of these minerals to the sediments is constant, and that detrital grains have invariant Ba/Al ratios, so that only changes in non-detrital Ba accumulation control changes in Ba/Al ratios (Paytan and Griffith, 2007). These latter assumptions, however, may not be valid for the studied core intervals because changes in the hydrological cycle resulted in large changes in the delivery of terrigenous material to the ocean during the PETM (Carmichael et al., 2017).

5.3. Isotopic constraints on the marine Ba cycle

To better constrain non-detrital Ba accumulation we introduce Ba isotope compositions as a new paleo-proxy. The transfer of dissolved Ba to particulate phases in the upper water column, predominantly due to $BaSO_4$ precipitation, is associated with an isotope fractionation with a preference for the lighter isotopes (Horner et al., 2015, 2017; Bates et al., 2017; Hsieh and Henderson, 2017; Bridgestock et al., 2018). The magnitude of this isotope fractionation is estimated to be $\Delta^{138/134}Ba_{Diss\text{-}Part} \approx 0.5‰$ based on comparison between the isotope composition of suspended particulate and underlying sedimentary Ba with upper-ocean dissolved Ba in the South Atlantic (Horner et al., 2017; Bridgestock et al., 2018). Deeper in the water column, this isotopically 'light' particulate Ba is partially regenerated to the dissolved pool, due to dissolution of $BaSO_4$ particles exported from above. This vertical cycling results in a strong negative correlation between dissolved Ba concentrations and $\delta^{138/134}$Ba values observed throughout the modern ocean (Fig. 4), with upper-ocean waters depleted in dissolved Ba, featuring higher $\delta^{138/134}$Ba values, and the deep ocean enriched in dissolved Ba, featuring lower $\delta^{138/134}$Ba values (Horner et al., 2015; Bates et al., 2017; Hsieh and Henderson, 2017; Bridgestock et al., 2018; Hemsing et al., 2018). It is possible that the exact relationship between dissolved Ba concentrations and isotope compositions may have changed over geological timescales, however we expect this qualitative description of Ba isotope cycling to be valid during the PETM.

Unlike indices of non-detrital Ba accumulation (i.e. BAR and Ba/Al ratios) the Ba isotopic signatures recorded by sediments should be insensitive to dilution effects and local changes in $BaSO_4$ preservation. The latter is based on the assumption that $BaSO_4$ dissolution in the deep ocean is not accompanied by an isotopic fractionation. Validation for this assumption is provided by the identical $\delta^{138/134}$Ba values (≈0.1‰) of suspended particulate Ba in the upper water column of the South Atlantic (Horner et al., 2017), and non-detrital Ba buried in underlying South Atlantic sediments (Bridgestock et al., 2018). These isotope compositions are also consistent with an estimate of the globally averaged $\delta^{138/134}$Ba value of Ba regenerated from sinking particles in the deep ocean (Bridgestock et al., 2018). Taken together, this suggests that no isotope fractionation accompanies partial $BaSO_4$ dissolution in the deep ocean, in accord with experimental evidence (von Allmen et al., 2010). The isotope composition of non-detrital Ba in marine sediments should therefore reflect the composition of particulate Ba exported from the overlying upper water column.

Away from continental margins, upper water-column dissolved Ba inventories are controlled by a balance between the supply of

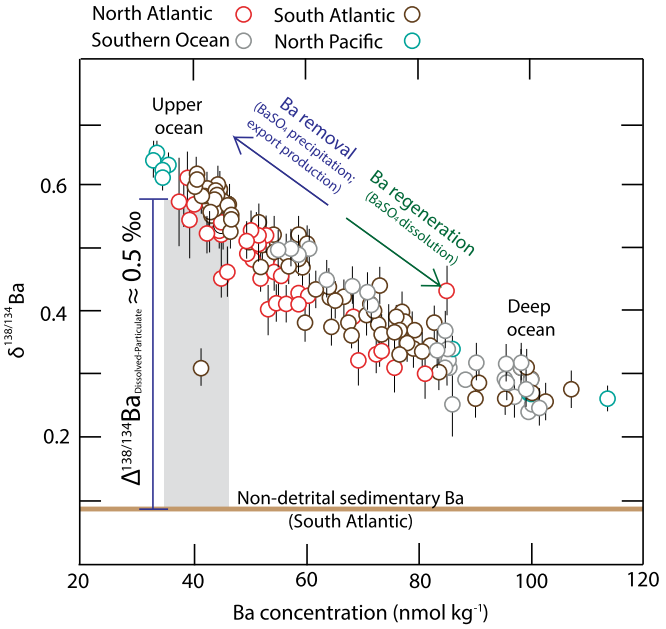

Fig. 4. Relationship between dissolved Ba concentrations and isotope compositions in the modern ocean (Horner et al., 2015; Bates et al., 2017; Hsieh and Henderson, 2017; Bridgestock et al., 2018; Hemsing et al., 2018). The horizontal brown line shows the isotope composition of non-detrital Ba in modern sediments from the South Atlantic (Bridgestock et al., 2018), which is consistent with those of suspended particulate Ba collected in the upper 1000 m of the South Atlantic water column (Horner et al., 2017; not shown). The offset between these sedimentary and particulate $\delta^{138/134}$Ba values to those of overlying upper ocean waters of 0.5‰ (shown by vertical grey band) represents the magnitude of the isotope fractionation accompanying Ba removal from upper-ocean waters.

Ba via lateral and upward advection/mixing, versus the removal of Ba by $BaSO_4$ precipitation, related to export production. To provide a useful framework to interpret coupled changes in non-detrital Ba accumulation and sediment $\delta^{138/134}$Ba values we use a simple steady state box model (Fig. 5), to derive the following equation ((4); Supplementary Information).

$$\delta^{138/134}Ba_{Part} = BAR \times (1/f_{pres})\left(\Delta^{138/134}Ba_{Diss\text{-}Part}/S\right) + \left(\delta^{138/134}Ba_{In} - \Delta^{138/134}Ba_{Diss\text{-}Part}\right) \quad (4)$$

The box model considers a region of the upper ocean, that has an input flux of dissolved Ba (S) of a certain isotope composition ($\delta^{138/134}Ba_{In}$) by a combination of upward (from the deep-ocean), and lateral (from adjacent regions of the upper ocean) advection and mixing (Fig. 5). This input flux (S) is balanced by the output flux, which is partitioned between sinking particles, and lateral/downward advection and mixing. The difference in isotope composition between the sinking particles ($\delta^{138/134}Ba_{Part}$) and dissolved Ba in the upper ocean is given by the fractionation factor ($\Delta^{138/134}Ba_{Diss\text{-}Part}$, ≈0.5‰). The flux of Ba exported from the upper ocean by sinking particles is observed to be proportional to export production in the modern ocean (e.g. Dymond et al., 1992), and BAR in underlying sediments represents the fraction of this flux that escapes dissolution in the deep ocean and gets buried (f_{pres}). Coupling records of BAR with sediment $\delta^{138/134}$Ba values may allow an approach to see through the problems of dissolution and dilution in use of BAR alone, and to obtain reliable interpretations of export production changes.

The isotope composition of the sinking particulate Ba flux ($\delta^{138/134}Ba_{Part}$), recorded by the sediment, should display linear, positive correlations with BAR if the following parameters remain constant with time: the fractionation factor ($\Delta^{138/134}Ba_{Diss\text{-}Part}$), Ba supply flux (S) and isotope composition ($\delta^{138/134}Ba_{In}$), and

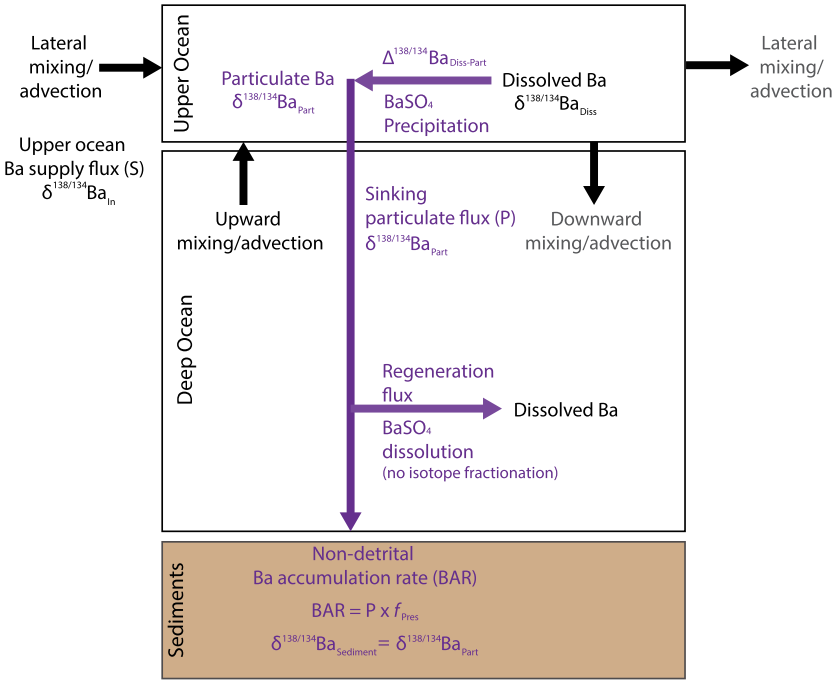

Fig. 5. Schematic of steady state box model used to develop a framework to interpret coupled records of non-detrital Ba accumulation and sediment $\delta^{138/134}$Ba values (4).

the preservation fraction (f_{pres}) (4). The gradient of this relationship would then be proportional to the fractionation factor ($\Delta^{138/134}Ba_{Diss\text{-}Part}$), and inversely proportional to the supply flux (S) and preservation fraction (f_{pres}) (Fig. 6; (4)). The y-intercept of this relationship depends on both the fractionation factor ($\Delta^{138/134}Ba_{Diss\text{-}Part}$) and the isotope composition of the supply flux ($\delta^{138/134}Ba_{In}$).

For a given region of the upper ocean, the supply flux of Ba and its isotope composition may vary temporally due to changes in ocean circulation, changes in Ba cycling in distal regions of the ocean or potentially whole ocean changes in Ba inventories. Whole ocean changes in Ba inventories may occur over timescales longer than the residence time of Ba in the ocean (~8 kyr), due to changes external inputs of Ba to the ocean (from rivers, hydrothermal vents and possibly also CH_4 cold seeps), or its output from the ocean, which is largely governed by export production and $BaSO_4$ preservation (Paytan and Kastner, 1996; Dickens et al., 2003). Such changes may have occurred across the studied PETM interval, which span ~200 kyrs (Murphy et al., 2010; Westerhold et al., 2018). Large changes in chemical inputs to the ocean, due to enhanced weathering and runoff, are thought to have occurred during the PETM (Carmichael et al., 2017), which may have impacted the marine Ba cycle. Furthermore, it has previously been proposed that the release of huge amounts of CH_4 from the seafloor during the PETM onset, a proposed source of ^{13}C depleted carbon to the ocean and atmosphere, may also have released large amounts of Ba to the ocean (Dickens et al., 2003). This may have raised the $BaSO_4$ saturation state of the whole ocean, resulting in higher non-detrital Ba accumulation rates due to globally higher preservation (f_{pres}). Constraints are currently unavailable to allow assessment of the exact impact of such whole ocean changes on marine Ba isotope inventories, however, they would be expected to change the flux (S) and isotope composition of ($\delta^{138/134}Ba_{In}$) of Ba supplied to specific regions of the upper ocean (4). Therefore the expected consequence would be to scatter sediment $\delta^{138/134}$Ba values and non-detrital Ba accumulation rates from a single linear relationship (Fig. 6).

The consistency of the relationship between dissolved Ba concentrations and isotope compositions observed throughout the modern ocean (Fig. 4) suggests that fractionation factor between dissolved and particulate phases ($\Delta^{138/134}Ba_{Diss\text{-}Part}$) is reasonably constant (Hsieh and Henderson, 2017; Bridgestock et al., 2018). The mechanism of the transfer of dissolved Ba to particulate phases in the upper ocean remains poorly understood however, and it is possible that the associated isotopic fractionation could vary under different conditions. Changes in the fractionation factor ($\Delta^{138/134}Ba_{Diss\text{-}Part}$) would also decouple relationships between BAR and sediment $\delta^{138/134}$Ba values, similar to changes in the supply flux (S) and isotope composition ($\delta^{138/134}Ba_{In}$) and preservation rate ((4); Fig. 6).

In summary, coupled records of non-detrital Ba accumulation rates and sediment $\delta^{138/134}$Ba values may allow assessment of the multiple controls on BAR (export production, dilution and $BaSO_4$ preservation), enabling reliable interpretation of export production reconstructions. Furthermore, such coupled records may also provide insights into the importance of local changes in export production, versus changes in ocean circulation, and distal or even whole ocean changes in marine Ba isotope cycling, and for controlling sediment $\delta^{138/134}$Ba values. Specifically, positive linear correlations between non-detrital Ba accumulation rates and sediment $\delta^{138/134}$Ba values would be consistent with both of these variables responding locally to export production. If changes in BAR are largely controlled by changing $BaSO_4$ preservation rates, or reflect dilution artifacts, BAR and sediment $\delta^{138/134}$Ba values would be expected to deviate from a single linear relationship (Fig. 6). Likewise, changes in the flux and isotope composition of Ba supplied to the overlying upper water column, or changes in the fractionation factor, would also be expected to cause BAR and sediment $\delta^{138/134}$Ba values to deviate from a single linear relationship.

5.4. Coupled sedimentary Ba isotope and Ba accumulation constraints on export production changes during the PETM

Changes in $\delta^{138/134}$Ba values following the onset of the PETM are positively correlated with BARs calculated using extraterrestrial ^{3}He and Ba/Al ratios at Site 690 ($r^2 = 0.38$ and 0.40) and 1263 ($r^2 = 0.72$ and 0.85) (Fig. 7). In contrast, there is no correlation observed at either site between $\delta^{138/134}$Ba values and BARs derived

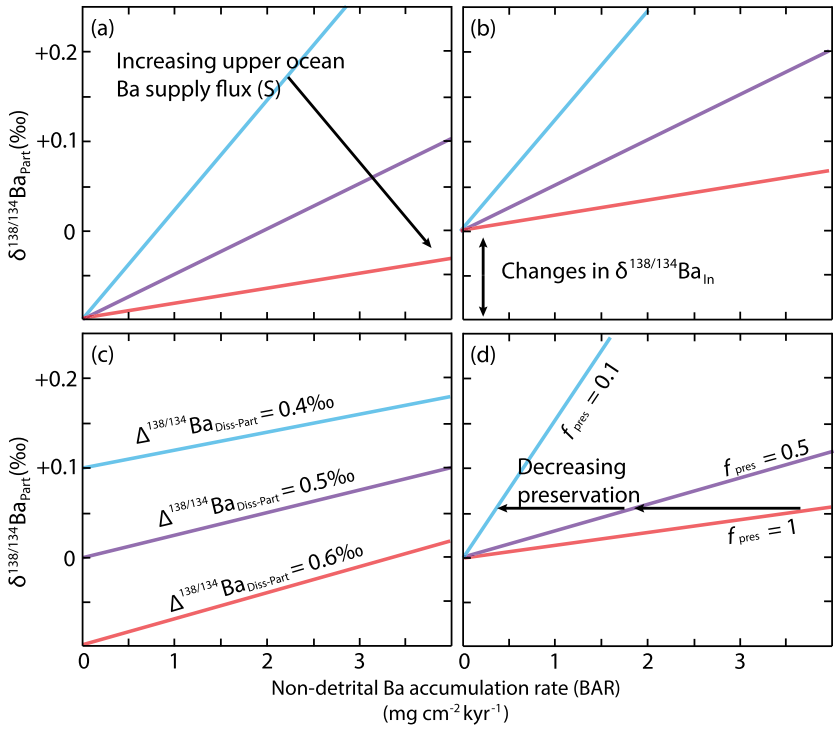

Fig. 6. Predicted relationships between the isotope composition ($\delta^{138/134}Ba_{Part}$) and the accumulation rate of non-detrital Ba in marine sediments (4). Panels (a) and (b) illustrate the expected effects of changing the flux (S) and isotope composition ($\delta^{138/134}Ba_{In}$) of dissolved Ba supplied to the overlying upper ocean via ocean circulation. Panel (c) illustrates the expected effects of changing the fractionation factor between dissolved and particulate Ba phases ($\Delta^{138/134}Ba_{Diss\text{-}Part}$) in the overlying upper ocean. Panel (d) illustrates the expected effect of changing the fraction of the sinking particulate flux that is preserved in marine sediments (f_{pres}).

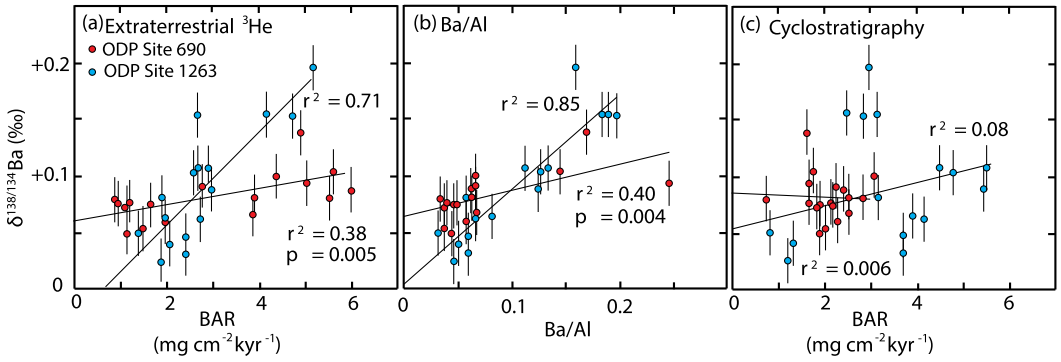

Fig. 7. Relationship between $\delta^{138/134}Ba$ values and indices of non-detrital Ba accumulation in sediments following the onset of the PETM. In panel (a), non-detrital Ba accumulation rates (BAR) are derived using sedimentation rates estimated using extraterrestrial ^3He (Farley and Eltgroth, 2003; Murphy, 2011). Panel (b) displays relationship between $\delta^{138/134}Ba$ values and Ba/Al ratios. In panel (c) non-detrital BARs derived using sedimentation rates estimated from cycle stratigraphy age models (Westerhold et al., 2018). For site 1263, the four samples immediately following the negative carbon isotope excursion which, based on measured Ba/Al ratios, feature significant Ba contributions from detrital sources, are omitted from the regression (Fig. 3).

using age models based on cyclostratigraphy (Fig. 7c). Barium isotope results therefore support the use of Ba/Al ratios and extraterrestrial ^3He to assess changes in Ba accumulation across the PETM at these sites. By extension these results also favor the use of the extraterrestrial ^3He (Farley and Eltgroth, 2003; Murphy et al., 2010; Murphy, 2011) over cyclostratigraphic age models (Westerhold et al., 2018) for assessing sedimentation rate changes occurring during the studied intervals.

The positive correlation between these indices of Ba accumulation and sedimentary $\delta^{138/134}Ba$ values are consistent with changes in export production rather than local or even global changes in $BaSO_4$ preservation, which would be expected to decouple these variables (Fig. 6; section 5.3). Furthermore, these records show maximum values of Ba accumulation occur during the recovery period, at least 10 to 30 kyrs after the hypothesized dissociation of methane hydrates would have ceased (Fig. 8; Zeebe et al., 2009). This time lag is significantly longer than the residence time of Ba in the ocean (~8 kyrs; Dickens et al., 2003), so is inconsistent with the proposed scenario that increased Ba accumulation is due to higher $BaSO_4$ preservation related to large scale dissolved Ba inputs at the PETM onset (Dickens et al., 2003). This agrees with evidence from Sr/Ba ratios of sedimentary $BaSO_4$ suggesting the $BaSO_4$ saturation state of the ocean did not change significantly during the PETM (Paytan et al., 2007).

The relationships between BAR (derived using extraterrestrial ^3He) and Ba/Al ratios with $\delta^{138/134}Ba$ values display gradients that are about ~4 to 6 times steeper at Site 1263 compared to Site 690 (Fig. 7). The y-intercept of the relationships from these two sites is also slightly different (≈0‰ for Site 1263, and ≈0.06‰ for Site 690). These differences in gradient may reflect different $BaSO_4$

preservation rates (f_{pres}), upper ocean Ba supply fluxes (S), or potentially different fractionation factors ($\Delta^{138/134}Ba_{Diss-Part}$) between the two sites (Fig. 6; (4)). The differences in y-intercept could reflect a higher $\delta^{138/134}$Ba value of the Ba supplied to the upper ocean at Site 690 compared to Site 1263, and/or differences in the fractionation factor (Fig. 6; (4)). The scatter observed in the relationships at both sites is likely to reflect variable $BaSO_4$ preservation rates, residual uncorrected dilution artifacts (affecting BAR and Ba/Al), and/or temporal changes in upper ocean Ba supply rate and isotope composition (affecting $\delta^{138/134}$Ba values). Temporal changes in the fractionation factor ($\Delta^{138/134}Ba_{Diss-Part}$; (4)) could cause the data to scatter from a linear positive correlation. Regardless, the observation that sediment $\delta^{138/134}$Ba values are correlated with BAR (based on ^{3}He) and Ba/Al ratios is consistent with export production in the overlying water column being a dominant control on these variables.

5.5. Implications for the PETM

The new constraints from coupled sediment $\delta^{138/134}$Ba values and non-detrital Ba accumulation rates suggest export production at the studied sites remained at similar levels or decreased following the onset of the PETM, before increasing to maximum values in the PETM recovery period (Fig. 8). These interpretations disagree with previous applications of the Ba proxy at these same sites, which suggest that export production increased following the onset of the PETM and declined during the recovery period (Bains et al., 2000; Ma et al., 2014). The non-detrital Ba accumulation rates for ODP Sites 690 and 1051 (North Atlantic) presented by Bains et al. (2000) are known to reflect dilution artifacts due to the cyclostratigraphic age models used to account for sedimentation rate changes (Torfstein et al., 2010). As previously mentioned (section 5.1), Ma et al. (2014) used a sequential leaching procedure to measure $BaSO_4$ concentrations in the sediments, which show large disagreements with non-detrital Ba concentrations presented in this study (Fig. 3). It is possible that this discrepancy reflects significant contributions of Ba from non-$BaSO_4$ phases in our record. The high total Ba concentrations of the studied sediments are however difficult to explain without significant $BaSO_4$ contributions, suggesting that previous $BaSO_4$ accumulation records (Ma et al., 2014) may be biased by yield issues (section 5.1).

Our interpreted changes in export production are in good agreement with evidence from biotic proxies available for Site 690, which suggest an increase in calcareous nannoplankton production during the recovery period (Bralower, 2002; Kelly et al., 2005; Gibbs et al., 2018). This is expected to be associated with an increase in production and export of particulate organic carbon in addition to biogenic carbonate (Gibbs et al., 2018), as supported by our Ba records (Fig. 8). An expected consequence of our inferred increase in export production would be deoxygenation of the overlying water column. Further validation of our interpretation is therefore provided by evidence of reduced bottom water oxygenation at both sites coinciding with the inferred increase in export production during the PETM recovery period (Chun et al., 2010; Pälike et al., 2014).

Increased export production during the recovery period may have been driven by increased nutrient supply due to cooling climate and decreasing ocean stratification (Winguth et al., 2012) and/or increased terrestrial runoff (Kelly et al., 2005; Carmichael et al., 2017). It coincides with an increase in sedimentation rates (based on ^{3}He; Fig. 2) and accumulation of biogenic carbonate at these sites (Kelly et al., 2005; Zachos et al., 2005; Farley and Eltgroth, 2003; Murphy, 2011) (Fig. 3; Fig. 8). This enhanced carbonate burial represents an important mode of carbon sequestration during the recovery from the PETM (Kelly et al., 2005; Zachos et al., 2005; Penman et al., 2016). The importance of increased production versus preservation for controlling this carbonate burial is uncertain (Kelly et al., 2005; Gibbs et al., 2010). Our presented interpretation of export production supports the important role of marine productivity for driving rapid carbon sequestration by carbonate burial during recovery from the PETM. In addition, this increase in export production likely contributed to water column deoxygenation (Chun et al., 2010; Pälike et al., 2014), and may have help create conditions conducive to increased organic carbon burial.

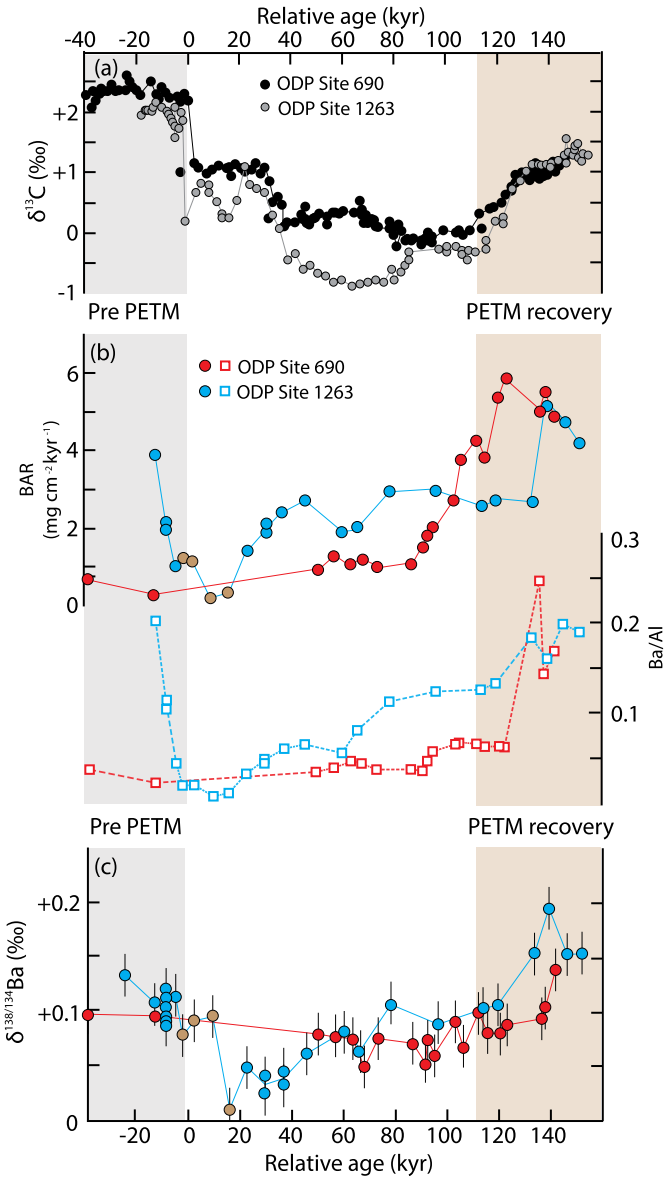

Fig. 8. Changes in bulk carbon isotope compositions, non-detrital Ba accumulation rates (BAR), Ba/Al ratios and Ba isotope compositions as a function of relative age across the PETM. Age models and BARs are based on extraterrestrial ^{3}He derived sedimentation rates (Farley and Eltgroth, 2003; Murphy, 2011; Supplementary Information).

6. Conclusions

This study presents a new approach using Ba isotopes variations to assess the multiple potential controls on sedimentary non-detrital Ba accumulation rates, allowing more robust reconstructions of export production. Positive linear correlations between sediment $\delta^{138/134}$Ba values and non-detrital Ba accumulation rates are consistent with both of these variables being controlled by

local changes in export production. Coupled records of sediment $\delta^{138/134}$Ba values and non-detrital Ba accumulation therefore allow assessment of dilution artifacts and $BaSO_4$ preservation changes that represent significant issues for the use of Ba accumulation rates to reconstruct export production.

Application of this approach to sediments deposited during the PETM reveals that export production remained unchanged or decreased following the onset of the PETM in the South Atlantic and Southern Ocean, before increasing during the recovery from the PETM. These interpretations disagree with previous applications of the Ba proxy (Bains et al., 2000; Ma et al., 2014), but are consistent with evidence provided by nannofossils (Bralower, 2002; Kelly et al., 2005; Gibbs et al., 2018). These findings help resolve uncertainty over the response of biological productivity to climate change experienced during the PETM, and support the important role of export production for carbon sequestration by driving carbonate burial during the rapid recovery from the PETM.

Acknowledgements

Samples were provided by the Integrated Ocean Drilling Program. We thank Phil Holdship for determining sediment Al concentrations by ICP-MS, and Gregory Brennecka for advice on Ba isotope analyses using a double filament assembly. Stuart Robinson is thanked for constructive discussions on this work. We also thank three anonymous reviewers for constructive comments that helped to greatly improve this manuscript. This work was supported by funding from Shell Global Solutions BV.

Appendix A. Supplementary material

Supplementary material related to this article can be found online at https://doi.org/10.1016/j.epsl.2018.12.036.

References

Bains, S., Corfield, R.M., Norris, R.D., 1999. Mechanisms of climate warming at the end of the Paleocene. Science 285, 724–727.

Bains, S., Norris, R.D., Corfield, R.M., Faul, K.L., 2000. Termination of the global warmth at the Palaeocene/Eocene boundary through productivity feedback. Nature 407, 101–174.

Bates, S.L., Hendry, K.R., Pryer, H.V., Kinsley, C.K., Pyle, K.M., Woodward, E.M., Horner, T.J., 2017. Barium isotopes reveal role of ocean circulation on barium cycling in the Atlantic. Geochim. Cosmochim. Acta 204, 286–299. https://doi.org/10.1016/j.gca.2017.01.043.

Bowen, G.J., Zachos, J.C., 2010. Rapid carbon sequestration at the termination of the Palaeocene–Eocene Thermal Maximum. Nat. Geosci. 3, 866–896. https://doi.org/10.1038/ngeo1014.

Bralower, T.J., 2002. Evidence of surface water oligotrophy during the Paleocene–Eocene thermal maximum: Nannofossil assemblage data from Ocean Drilling Program Site 690, Maud Rise, Weddell Sea. Paleoceanography 17, 1023. https://doi.org/10.1029/2001PA000662.

Bridgestock, L., Hsieh, Y-T., Porcelli, D., Homoky, W.B., Bryan, A., Henderson, G.M., 2018. Controls on the barium isotope compositions of marine sediments. Earth Planet. Sci. Lett. 481, 101–110. https://doi.org/10.1016/j.epsl.2017.10.019.

Carmichael, M.J., et al., 2017. Hydrological and associated biogeochemical consequences of rapid global warming during the Paleocene–Eocene Thermal Maximum. Glob. Planet. Change 157, 114–138. https://doi.org/10.1016/j.gloplacha.2017.07.014.

Chun, C.O.J., Delaney, M.L., Zachos, J.C., 2010. Paleoredox changes across the Paleocene–Eocene thermal maximum, Walvis Ridge (ODP Sites 1262, 1263, and 1266): evidence from Mn and U enrichment factors. Paleoceanography 25. https://doi.org/10.1029/2009PA001861.

Dehairs, F., Chesselet, R., Jebwab, J., 1980. Discrete suspended particles of barite and the barium cycle in the open ocean. Earth Planet. Sci. Lett. 49, 528–550.

Dickens, G.R., Fewless, T., Thomas, E., Bralower, T.J., 2003. Excess barite accumulation during the Paleocene–Eocene Thermal Maximum: massive input of dissolved barium from seafloor gas hydrate reservoirs. In: Ginerich, P., et al. (Eds.), Causes and Consequences of Globally Warm Climates in the Early Paleogene. In: Geological Society of America Special Paper, vol. 369, pp. 11–23.

Dickens, G.R., O'Neil, J.R., Rea, D.K., Owen, R.M., 1995. Dissociation od oceanic methane hydrate as a cause of the carbon isotope excursion at the end of the Paleocene. Paleoceanogr. Curr. 10, 965–971.

Dunkley Jones, T., Lunt, D.J., Schmidt, D.N., Ridgwell, A., Sluijs, A., Valdes, P.J., Maslin, M., 2013. Climate model and proxy data constraints on ocean warming across the Paleocene–Eocene Thermal Maximum. Earth-Sci. Rev. 125, 123–145. https://doi.org/10.1016/j.earscirev.2013.07.004.

Dymond, J., Suess, E., Lyle, E., 1992. Barium in deep-sea sediment: a geochemical proxy for paleoproductivity. Paleoceanography 7 (2), 163–181.

Eagle, M., Paytan, A., Arrigo, K.R., van Dijken, G., Murray, R.W., 2003. A comparison between excess barium and barite as indicators of carbon export. Paleoceanography 18 (1), 1021. https://doi.org/10.1029/2002PA000793.

Fagel, N., Dehairs, F., Andre, L., Bareille, G., Monnin, C., 2002. Ba distribution in surface Southern Ocean sediments and export production estimates. Paleoceanography 17 (2), 1011. https://doi.org/10.1029/2000PA000552.

Farley, K.A., Eltgroth, S.F., 2003. An alternative age model for the Paleocene–Eocene thermal maximum using extraterrestrial ^{3}He. Earth Planet. Sci. Lett. 208, 135–148. https://doi.org/10.1016/S00012-821X(03)00017-7.

Gibbs, S.J., Bralower, T.J., Bown, P.R., Zachos, J.C., Bybell, L.M., 2006. Shelf and open-ocean calcareous phytoplankton assemblages across the Paleocene–Eocene Thermal Maximum: implications for productivity gradients. Geology 34, 233–236. https://doi.org/10.1130/G22381.1.

Gibbs, S.J., Sheward, R., Brown, P.R., Poulton, A.J., Alvarex, S.A., 2018. Warm plankton soup and red herrings: calcareous nannoplankton cellular communities and the Palaeocene–Eocene Thermal Maximum. Philos. Trans. A 376. https://doi.org/10.1098/rsta.2017.0075.

Gibbs, S.J., Stoll, H.M., Bown, P.R., Bralower, T.J., 2010. Ocean acidification and surface water carbonate production across the Paleocene–Eocene thermal maximum. Earth Planet. Sci. Lett. 295, 583–592. https://doi.org/10.1016/j.epsl.2010.04.044.

Gonneea, M.E., Paytan, A., 2006. Phase associations of barium in marine sediments. Mar. Chem. 100, 124–135.

Gutjahr, M., Ridgwell, A., Sexton, P.F., Anagnostou, E., Pearson, P.N., Pälike, H., Norris, R.D., Thomas, E., Foster, G.L., 2017. Very large release of mostly volcanic carbon during the Palaeocene–Eocene Thermal Maximum. Nature 548, 572–577. https://doi.org/10.1038/nature23646.

Hemsing, F., Hsieh, Y-T., Bridgestock, L., Spooner, P.T., Robinson, L.F., Frank, N., Henderson, G.M., 2018. Barium isotopes in cold-water corals. Earth Planet. Sci. Lett. 491, 183–192. https://doi.org/10.1016/j.epsl.2018.03.040.

Homoky, W.B., Hembury, D.J., Hepburn, L.E., Mills, R.A, Statham, P.J., Fones, G., Palmer, M., 2011. Iron and manganese diagenesis in deep sea volcanogenic sediments and the origins of pore water colloids. Geochim. Cosmochim. Acta 75, 5032–5048. https://doi.org/10.1016/j.gca.2011.06.019.

Horner, T.J., Kinsley, C.W., Nielsen, S.G., 2015. Barium-isotopic fractionation in seawater mediated by barite cycling and oceanic circulation. Earth Planet. Sci. Lett. 430, 511–522. https://doi.org/10.1016/j.epsl.2015.07.027.

Horner, T.J., Pryer, H.V., Nielsen, S.G., Crockford, P.W., Gauglitz, J.M., Wing, B.A., Ricketts, R.D., 2017. Pelagic barite precipitation at micromolar ambient sulfate. Nat. Commun. 8, 1242. https://doi.org/10.1038/s41467-017-01229-5.

Hsieh, Y-T., Henderson, G.M., 2017. Barium stable isotopes in the global ocean: tracer of Ba inputs and utilization. Earth Planet. Sci. Lett. 473, 269–278. https://doi.org/10.1016/j.epsl.2017.06.024.

Kelly, D.C., Zachos, J.C., Bralower, T.J., Schellenberg, S.A., 2005. Enhanced terrestrial weathering/runoff and surface ocean carbonate production during the recovery stages of the Paleocene–Eocene thermal maximum. Paleoceanography 20, PA4023. https://doi.org/10.1029/2005PA001163.

Klump, J., Hebbeln, D., Wefer, G., 2000. The impact of sediment provenance on barium-based productivity estimates. Mar. Geol. 169, 259–271.

Komar, N., Zeebe, R.E., 2017. Redox-controlled carbon and phosphorus burial: a mechanism for enhanced organic carbon sequestration during the PETM. Earth Planet. Sci. Lett. 479, 71–82. https://doi.org/10.1016/j.epsl.2017.09.011.

Lea, D., Boyle, E., 1989. Barium content of benthic foraminifera controlled by bottom-water composition. Nature 318 (6218), 751–753.

Ma, Z., Gray, E., Thomas, E., Murphy, B., Zachos, J., Paytan, A., 2014. Carbon sequestration during the Palaeocene–Eocene Thermal Maximum by an efficient biological pump. Nat. Geosci. 7, 382–388. https://doi.org/10.1038/NGEO2139.

McInerney, F.A., Wing, S.L., 2011. The Paleocene–Eocene Thermal Maximum: a perturbation of carbon cycle, climate, and biosphere with implications for the future. Annu. Rev. Earth Planet. Sci. 39, 489–516. https://doi.org/10.1146/annurev-earth-040610-133431.

Murphy, B.H., 2011. Insights Into the Pace and Paleoceanography of Early Eocene Events of Global Warming. Ph.D. Thesis. University of California, Santa Cruz.

Murphy, B.H., Farley, K.A., Zachos, J.C., 2010. An extraterrestrial ^{3}He-based timescale for the Paleocene–Eocene thermal maximum (PETM) from Walvis Ridge, IODP site 1266. Geochim. Cosmochim. Acta 74, 5098–5108. https://doi.org/10.1016/j.gca.2010.03.039.

Nan, X., Yu, H-M., Rudnick, R.L., Gasching, R.M., Xu, J., Li, W-Y., Zhang, Q., Jin, Z-D., Li, X-H., Huang, F., 2018. Barium isotopic composition of the upper continental crust. Geochim. Cosmochim. Acta 233, 33–49. https://doi.org/10.1016/j.gca.2018.05.004.

Pälike, C., Delaney, M.L., Zachos, J.C., 2014. Deep-sea redox across the Paleocene–Eocene thermal maximum. Geochem. Geophys. Geosyst. 15, 1038–1053. https://doi.org/10.1002/2013GC005074.

Paytan, A., Averyt, K., Faul, K., Gray, E., Thomas, E., 2007. Barite accumulation, ocean productivity, and Sr/Ba in barite across the Paleocene–Eocene Thermal Maximum. Geology 35, 1139–1142. https://doi.org/10.1130/G24162A.1.

Paytan, A., Griffith, E.M., 2007. Marine barite: recorder of variations in ocean export productivity. Deep-Sea Res. II 54, 687–705. https://doi.org/10.1016/j.dsr2.2007.01.007.

Paytan, A., Kastner, M., 1996. Benthic Ba fluxes in the central Equatorial Pacific, implications for the oceanic Ba cycle. Earth Planet. Sci. Lett. 142, 439–450.

Penman, D.E., Kirtland Turner, S., Sexton, P.F., Norris, R.D., Dickson, A.J., Boulila, S., Ridgwell, A., Zeebe, R.E., Zachos, J.C., Cameron, A., Westerhold, T., Röhl, U., 2016. An abyssal carbonate compensation depth overshoot in the aftermath of the Palaeocene–Eocene Thermal Maximum. Nat. Geosci. 9, 575–580. https://doi.org/10.1038/ngeo2757.

Reitz, A., Pfeifer, K., de Lange, G.J., Klump, J., 2004. Biogenic barium and the detrital Ba/Al ratio: a comparison of their direct and indirect determination. Mar. Geol. 204, 289–300. https://doi.org/10.1016/S0025-3227(04)00004-0.

Rutten, A., de Lange, G.J., 2002. A novel selective extraction of barite, and its application to eastern Mediterranean sediments. Earth Planet. Sci. Lett. 198, 11–24.

Stoll, H.M., Shimizu, N., Archer, D., Ziveri, P., 2007. Coccolithophore productivity response to the greenhouse event of the Paleocene–Eocene Thermal Maximum. Earth Planet. Sci. Lett. 258, 192–206. https://doi.org/10.1016/j.epsl.2007.03.037.

Torfstein, A., Winckler, G., Tripati, A., 2010. Productivity feedback did not terminate the Paleocene–Eocene Thermal Maximum (PETM). Clim. Past 6, 266–272. https://doi.org/10.5194/cp-6-265-2010.

van Zuilen, K., Nägler, T.F., Bullen, T.D., 2016. Barium isotopic compositions of geological reference materials. Geostand. Geoanal. Res. 40, 543–558. https://doi.org/10.1111/ggr.12122.

von Allmen, K., Böttcher, M.E., Samankassou, E., Nägler, T.F., 2010. Barium isotope fractionation in the global barium cycle: first evidence from barium minerals and precipitation experiments. Chem. Geol. 277, 70–77. https://doi.org/10.1016/j.chemgeo.2010.07.011.

Westerhold, T., Röhl, U., Wilkens, R.H., Gingerich, P.D., Clyde, W.C., Wing, S.L., Bowen, G.J., Kraus, M.J., 2018. Synchronizing early Eocene deep-sea and continental records – cyclostratigraphic age models for the Bighorn Basin Coring Project drill cores. Clim. Past 14, 303–319. https://doi.org/10.5194/cp-14-303-2018.

Winguth, A.M.E., Thomas, E., Winguth, C., 2012. Global decline in ocean ventilation, oxygenation, and productivity during the Paleocene–Eocene Thermal Maximum: implications for the benthic extinction. Geology 40, 263–266. https://doi.org/10.1130/GS32529.1.

Zachos, J.C., et al., 2005. Rapid acidification of the ocean during the Paleocene–Eocene thermal maximum. Science 308, 1611–1615. https://doi.org/10.1126/science.1109004.

Zeebe, R.E., Zachos, J.C., Dickens, G.R., 2009. Carbon dioxide forcing alone insufficient to explain Palaeocene–Eocene Thermal Maximum warming. Nat. Geosci. 13, 576–580. https://doi.org/10.1038/NGEO578.